Plant Molecular Biology (2026) 116:52
https://doi.org/10.1007/s11103-026-01720-y

RESEARCH

Epigenetically regulated transcriptional repressor, BASIC PENTACYSTEINE1 (BPC1) acts together with polycomb repressive complex 2 (PRC2) to suppress camalexin biosynthesis in *Arabidopsis*

Heewon Moon[1] · Dasom Choi[1] · Eojin Cho[1] · Hyunjoon Kim[1] · Adji Baskoro Dwi Nugroho[1,2] · Dong-Hwan Kim[1]

Received: 30 January 2026 / Accepted: 25 April 2026 / Published Online: 13 May 2026

Abstract

Camalexin is a phytoalexin produced by plants of the Brassicaceae family, including the model species *Arabidopsis thaliana*, and its biosynthesis is tightly regulated to balance growth and defense. Here, we identify BASIC PENTACYSTEINE 1 (BPC1) as a key negative regulator of camalexin biosynthesis. Transcriptome analyses of *bpc1-1* and *bpc1-1;bpc2-1* mutants revealed both distinct and overlapping functions of BPC1 and BPC2, with BPC1-specific differentially expressed genes being highly enriched for camalexin biosynthetic processes. Consistently, multiple camalexin pathway genes were upregulated in *bpc1-1*, leading to increased camalexin accumulation. Analysis of publicly available ChIP-seq data together with mutant expression profiles showed that several BPC1-regulated camalexin biosynthetic genes are enriched for the repressive histone mark, H3K27me3 and are de-repressed in Polycomb Repressive Complex 2 (PRC2) mutants, indicating PRC2-dependent transcriptional silencing. ChIP–qPCR analyses further demonstrated that BPC1 directly binds GA-rich cis-elements in camalexin pathway genes, including *CYP71A12* and *CYP71B15*. Furthermore, epigenome profiling showed that the *BPC1* locus itself is embedded within an active chromatin environment enriched in H3K4me2/3, H3K36me3, and histone acetylation. Loss-of-function mutants of histone H3 methyltransferases like *ATX1*, *ATX2*, *ATXR7*, and *EFS* exhibited reduced *BPC1* expression, whereas a knock-out mutant of a histone H3 acetyltransferase gene, *HDA9*, *hda9-1* displayed elevated H3ac levels and increased *BPC1* transcript abundance, indicating that *BPC1* transcription is epigenetically modulated by both histone methylation and acetylation dynamics. Together, our findings establish BPC1 as an epigenetically regulated transcriptional repressor that partners with PRC2 to suppress camalexin biosynthesis, revealing a previously unrecognized regulatory module controlling the *basal* suppression of specialized defensive metabolism in Arabidopsis.

Key message

BPC1 directly binds GA-rich cis-elements in camalexin biosynthetic genes and recruits PRC2-mediated H3K27me3 silencing to suppress their expression. BPC1 transcription itself is epigenetically modulated by histone methylation and acetylation, establishing a previously unrecognized chromatin regulatory module that controls basal suppression of defensive metabolism in *Arabidopsis*.

Keywords BPC1 · Camalexin · Polycomb repressive complex 2 (PRC2) · H3K27me3 · transcriptome · Epigenetic regulation

Heewon Moon and Dasom Choi contributed equally to this work.

✉ Dong-Hwan Kim
dhkim92@cau.ac.kr

[1] Department of Plant Science and Technology, College of Biotechnology, Chung-Ang University, Anseong, Gyeonggi-do 17546, Republic of Korea

[2] Department of Agronomy, Faculty of Agriculture, Universitas Gadjah Mada, Sleman, Yogyakarta 55281, Indonesia

Introduction

Camalexin is a sulfur-containing secondary metabolite involved in the plant defense against biotic stresses like fungal and bacterial infection (Glawischnig 2007). The biosynthetic pathway of camalexin has been extensively characterized through genetic and biochemical studies (Fig. 1).

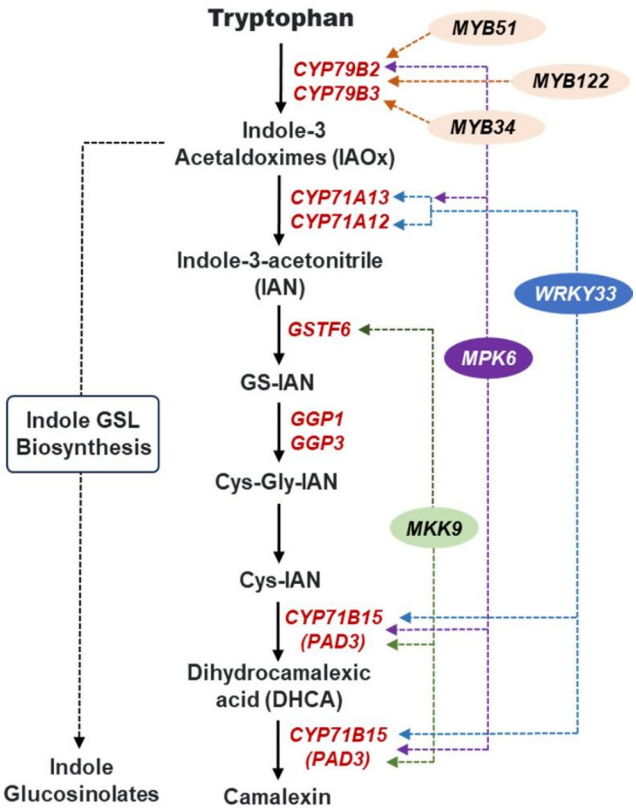

Fig. 1 A schematic diagram showing camalexin biosynthesis. Camalexin is derived from tryptophan which is firstly converted to indole-3-acetaldoxime (IAOx) by the cytochrome P450 enzymes CYP79B2 and CYP79B3. IAOx is then converted to indole-3-acetonitrile (IAN) by the CYP71A12 and CYP71A13 enzymes. Subsequently, IAN is converted to the Cys(IAN) conjugate after intermediate steps mediated by GSTF6, GGP1, and GGP3. The final two steps from Cys-IAN to camalexin biosynthesis are catalyzed by the P450 enzyme CYP71B15/PAD3.Three MYB domain proteins such as MYB34, MYB51, and MYB122 act to promote expression of upstream biosynthetic genes (*CYP79B2* and *CYP79B3*). A WRKY domain transcription factor, WRKY33 acts to promote expression of downstream biosynthetic genes (*CYP71A12*, *CYP71A13*, and *CYP71B15*). Two signaling factors like MKK9 and MPK6 play a positive role in the catalytic activity of GSTF6 and CYP71B15/PAD3 in the camalexin biosynthetic pathway of Arabidopsis

Tryptophan is first converted to indole-3-acetaldoxime (IAOx) by the cytochrome P450 enzymes CYP79B2 and CYP79B3. IAOx is then dehydrated to indole-3-acetonitrile (IAN) through the activities of CYP71A12 and CYP71A13 (Nafisi et al. 2007; Millet et al. 2010; Saga et al. 2012). Subsequent conjugation of IAN to glutathione, catalyzed by GSTF6, produces GS–IAN (Su et al. 2011), which is further processed by the γ-glutamyl peptidases GGP1 and GGP3 (Geu-Flores et al. 2011). Finally, the cytochrome P450 enzyme CYP71B15/PAD3 converts Cys–Glu–IAN to camalexin, completing the pathway (Zhou et al. 1999; Schuhegger et al. 2006; Bottcher et al. 2009).

BASIC PENTACYSTEINE (BPC) proteins, which contain a conserved GAGA-binding domain, are widely conserved across monocot and dicot species (Sangwan and O'Brian 2002; Santi and Schmidt 2009; Monfared et al. 2011; Simonini et al. 2012; Hecker et al. 2015; Shanks et al. 2018; Theune et al. 2019). In *Arabidopsis*, the BPC family comprises seven members classified into three subfamilies: class I (BPC1-BPC3), class II (BPC4-BPC6), and class III (BPC7) (Monfared et al. 2011; Meister et al. 2004). Higher-order *bpc* mutants exhibit severe developmental abnormalities including dwarfism, leaf curling, aberrant ovules, and reduced lateral root initiation, indicating that BPC proteins play essential roles in plant growth and organogenesis (Monfared et al. 2011). BPCs encode GAGA-binding domain which was shown to recognize and bind GA-rich motif and GA variants (RGARAGRRA consensus sequence) to regulate their downstream target genes (Xiao et al. 2017; Monfared et al. 2011; Simonini et al. 2012; Hecker et al. 2015; Shanks et al. 2018; Theune et al. 2019).

Epigenetic regulation is a key determinant of transcriptional control in eukaryotes. In plants, the Polycomb Repressive Complexes PRC1 and PRC2 mediate stable gene silencing primarily through the deposition and maintenance of H3K27me3 (Blackledge and Klose 2021). Mutations in PRC2 components such as *CLF* (*CURLY LEAF*), *LHP1* (*LIKE-HETEROCHROMATIN PROTEIN 1*), and *EMF1* (*EMBRYONIC FLOWER 1*) severely disrupt H3K27me3 patterns, leading to dramatic developmental defects like curled leaf, dwarfism, reduced sterility, and deformed floral organs (Schubert et al. 2006; Shu et al. 2019). Also, the deposition of H3K27me3 was severely damaged in *lhp1-4* and *emf1-1* mutant (Merini and Calonje 2015; Molitor et al. 2014; Kim et al. 2012; Turck et al. 2007). Studies suggested that LHP1 and EMF1, two PRC2 components are essentially required for stable maintenance of PRC2-mediated H3K27me3 on target genes.

Previously, it was reported that some BPCs associated with PRC2 and PRC1 complex to achieve stable suppression of *ABI4* (*ABA-INSENSITIVE 4*) to modulate lateral root formation (Mu et al. 2017). BPC6 was shown to interact with LHP1, a PRC2 component for suppression of homeotic genes in *Arabidopsis* (Hecker et al. 2015). Another study reported that BPCs including BPC1 acts as a repressor of the ovule identity gene, *SEEDSTICK* (*STK*) via direct binding to GA–rich boxes within the promoter region of *STK* (Kooiker et al. 2005; Petrella et al. 2020). These data indicated that BPCs, plant GAGA binding factors are involved in the recruitment of PRC2 complex via direct recognition of GAGA motifs in plants.

Though BPCs are considered to play an important role in many aspects of plant growth and development, function role of BPC family members are not fully explored. In this

study, we investigated the roles of *BPC1* and its close homolog *BPC2* through transcriptome profiling of *bpc1-1* and *bpc1-1;bpc2-1* mutants. Our analyses revealed that *BPC1* specifically represses camalexin biosynthetic genes, while *BPC2* displays a distinct regulatory signature. We further demonstrate that BPC1 directly binds GA-rich sequences in key camalexin pathway genes and cooperates with PRC2 to mediate their H3K27me3-dependent gene suppressions. Additionally, we show that *BPC1* transcription is itself epigenetically regulated through active histone modifications and the action of chromatin-modifying enzymes, including EFS (EARLY FLOWERING IN SHORT DAYS) and HDA9 (HISTONE DEACETYLASE 9). Together, these findings establish BPC1 as an epigenetically regulated transcriptional repressor that modulates camalexin biosynthesis through direct coordination with PRC2 complex, revealing a new regulatory layer controlling the basal suppression of specialized defensive metabolism under non-stress/non-inducing conditions in *Arabidopsis*.

Results

Transcriptome analysis suggested that BPC1 is involved in the control of camalexin biosynthesis

BASIC PENTACYSTEINE (BPC) proteins, which contain a GAGA-binding domain, constitute a small family of plant-specific transcription factors. This family comprises seven members and is classified into three groups: group I (*BPC1-BPC3*), group II (*BPC4-BPC6*), and group III (*BPC7*). Among these, BPC1 and BPC2 are the most closely related members (Supplementary Fig. S1). To investigate the functional roles of BPC1 and its closest homolog BPC2, we performed RNA sequencing (RNA-seq) analysis using two-week-old seedlings of wild-type Col-0, *bpc1-1*, and *bpc1-1;bpc2-1* mutants. Multidimensional scaling (MDS) analysis of the RNA-seq data revealed tight clustering of biological replicates within each genotype, indicating high-quality library preparation and robust transcriptomic data (Fig. 2A). Comparative transcriptome analyses identified 815 and 1,522 differentially expressed genes (DEGs) between Col-0 and *bpc1-1*, and between Col-0 and *bpc1-1;bpc2-1*, respectively (Fig. 2B and Supplementary Fig. S2).

Gene ontology (GO) enrichment analyses were subsequently performed for each DEG dataset to characterize the biological processes associated with BPC1 and BPC2 function (Fig. 2C and D). GO analysis using DEGs identified from the Col-0 versus *bpc1-1* comparison revealed significant enrichment of 'camalexin biosynthetic processes' among the top 10 GO categories (Fig. 2C), indicating that BPC1 plays a specific regulatory role in controlling camalexin biosynthesis. In contrast, GO analysis of DEGs derived from the Col-0 versus *bpc1-1;bpc2-1* double mutant comparison did not yield camalexin biosynthetic processes within the top 10 enriched GO categories (Fig. 2D). Instead, GO terms such as 'defense response to insect,' 'response to ozone,' and 'ATP synthesis' were predominantly represented, suggesting that the additional loss of BPC2 in the *bpc1-1* mutant background leads to broader and more complex transcriptomic changes that may mask or override the BPC1-specific regulatory signature observed in the single mutant. Collectively, these results suggest that BPC1 and BPC2 might have distinct yet partially overlapping regulatory functions, with BPC1 playing a more specific role in the suppression of camalexin biosynthetic genes. We note that RNA-seq data for the *bpc2-1* single mutant were not generated in the current study; transcriptome analysis of the *bpc2-1* single mutant would be required to fully resolve the individual transcriptional contributions of BPC2, and this is considered an important direction for future investigation.

Camalexin biosynthetic genes are upregulated in *bpc1-1* mutant compared to Col-0 under non-stress/non-inducing conditions

Because GO terms using *bpc1*-specific genes were mainly related to the regulation of camalexin biosynthesis, we examined the normalized transcript levels of camalexin pathway genes between Col-0 and *bpc1-1* mutant. Camalexin pathway genes were substantially upregulated in *bpc1-1* compared to Col-0. For instance, expression of six genes (*WRKY33*, *MYB51*, *MKK9*, *GSTF6*, *CYP71A12*, *CYP71B15/PAD3*) out of total 13 camalexin pathway genes were substantially higher in *bpc1-1* than those of Col-0 (Fig. 3A~3B). To validate RNA-seq data, we also performed real-time RT-PCR analysis between Col-0 and *bpc1-1* mutant. Similar to RNA-seq result, transcript levels of camalexin pathway genes were significantly higher in *bpc1-1* mutant compared to Col-0 (Fig. 3C). It indicated that BPC1 plays a suppressive role in the expression of camalexin biosynthetic genes under non-stress/non-inducing conditions in *Arabidopsis*. Next, we measured amounts of camalexin between Col-0 and *bpc1-1* mutant. In a consistency with RNA-seq and RT-qPCR data, camalexin was more accumulated in *bpc1-1* mutant than that of Col-0 (Fig. 3D). Altogether, these data indicated that BPC1 is involved in the suppression of camalexin biosynthesis under non-stress/non-inducing conditions in *Arabidopsis*.

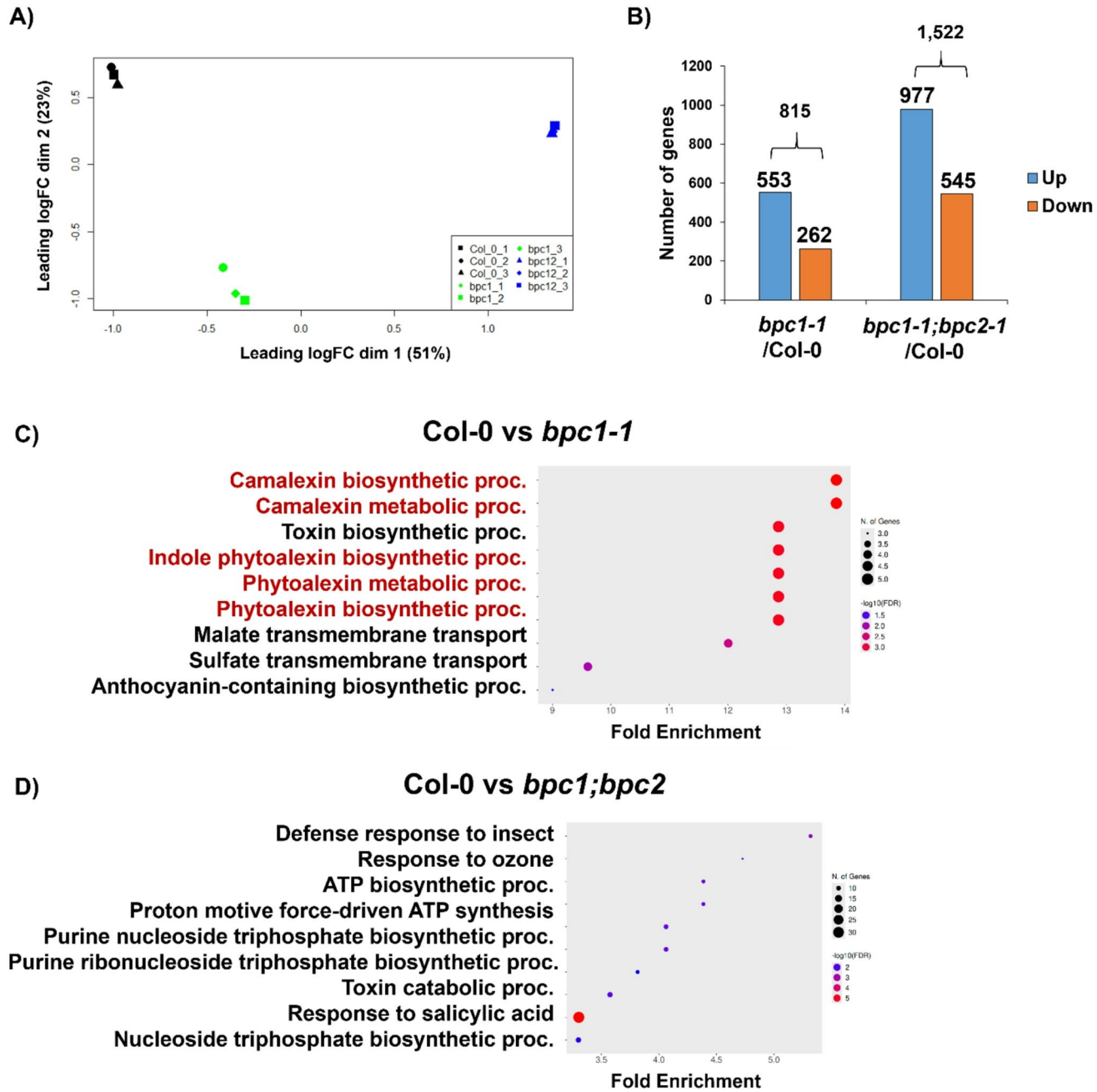

Fig. 2 Transcriptome analysis between Col-0, *bpc1-1*single mutant, and the*bpc1-1;bpc2-1*double mutant seedlings. **A** RNA-seq libraries were constructed and sequenced from three independent biological replicates of Col-0, *bpc1-1*, and *bpc1-1;bpc2-1* mutants. multi-dimensional scaling (MDS) plot was generated using R packages (ver. 3.6.0) (https://www.R-project.org/). Three different samples exhibited distin ct grouping of RNA-seq transcript profiles, indicating that RNA-seq library constructions and sequencings were well processed. **B** Number of differentially expressed genes (DEGs) in the *bpc1-1* mutant or the *bpc1-1;bpc2-1* double mutant compared to those of Col-0 wild type plant. Total 815 differentially expressed genes (DEGs) and 1,522 DEGs in the *bpc1-1* single mutant and the *bpc1-1;bpc2-1* double mutant were respectively detected compared to those of Col-0. **C** Result of gene ontology (GO) analysis using 815 differentially expressed genes (DEGs) in the *bpc1-1* single mutant compared to those of Col-0. Phytoalexin biosynthetic processes including camalexin were significantly represented in the the *bpc1-1* vs. Col-0 comparison. **D** Result of gene ontology (GO) analysis using 1,522 DEGs in the *bpc1;bpc2* mutant compared to those of Col-0. GO terms such as 'defense response to insect,' 'response to ozone,' and 'ATP synthesis' were predominantly represented, suggesting that the additional loss of BPC2 in the *bpc1-1* background might lead to broader transcriptomic changes that may mask or override the BPC1-specific regulatory signature. ShinyGO (ver 0.85) web-based tool was used for GO analysis in this study

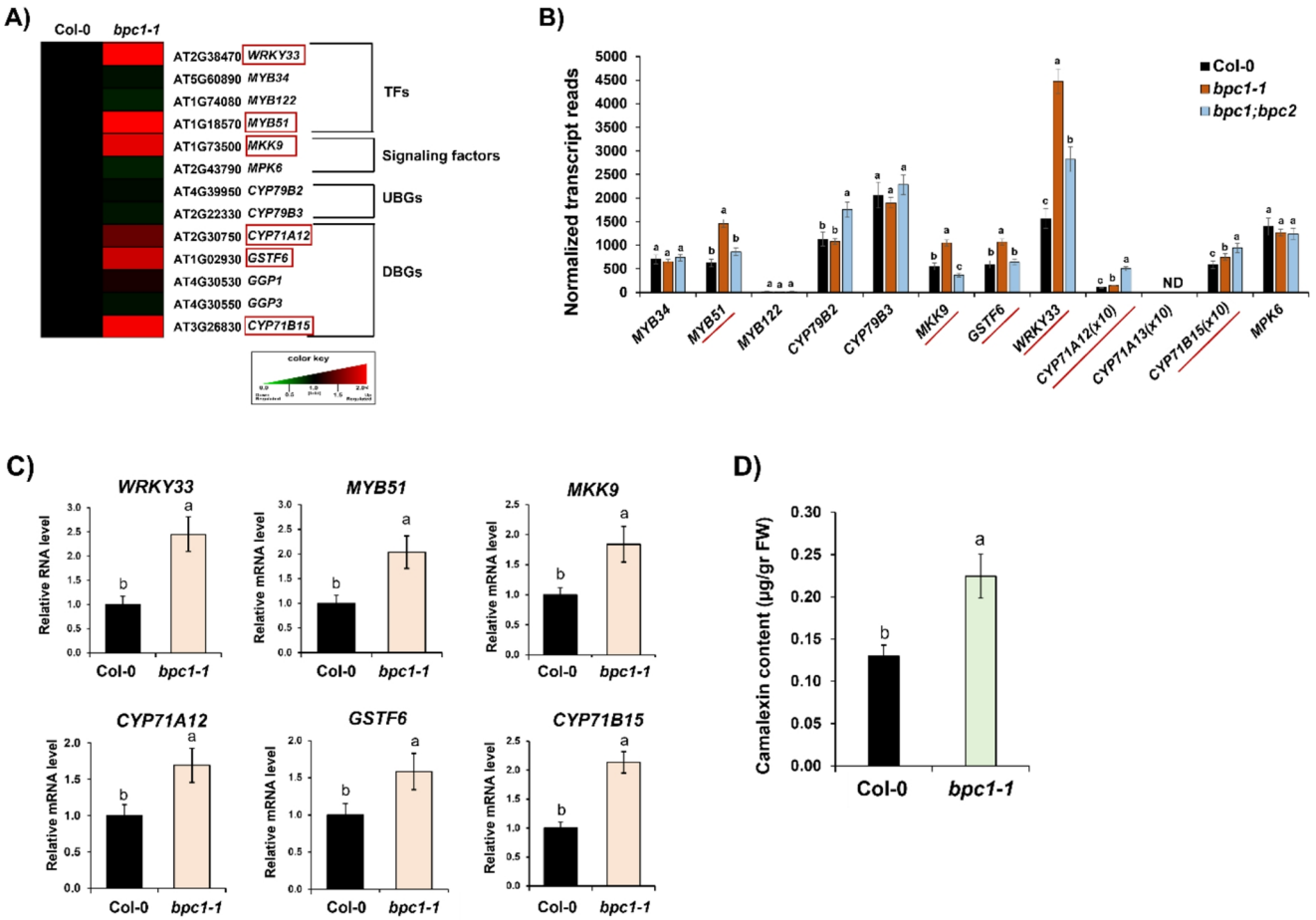

Fig. 3 BPC1 acts to suppress genes involved in the camalexin biosynthetic process in Arabidopsis. **A** Heatmap showing normalized RNA-seq transcript reads of four TF genes (*WRKY33*, *MYB34*, *MYB122*, and *MYB51*), two signaling genes (*MKK9* and *MPK6*), two upstream biosynthetic genes (*CYP79B2* and *CYP79B3*), and five downstream biosynthetic genes (*CYP71A12*, *GSTF6*, *GGP1*, *GGP3*, and *PAD3/CYP71B15*) between Col-0 and the *bpc1-1* mutant. Green to red color represents low to high transcript levels. **B** Bar graph showing normalized RNA-seq transcript reads of 12 camalexin pathway genes between Col-0 and the *bpc1-1* mutant. **C** Result of qRT-PCR analysis of six camalexin biosynthetic process genes between Col-0 and *bpc1-1* mutant. One-way ANOVA was applied to calculate the statistical significance, and significant difference was indicated in the figures by different letters ($p<0.05$). **D** Quantification of camalexin compound between Col-0 and the *bpc1-1* mutant. One-way ANOVA was applied to calculate the statistical significance, and significant difference was indicated above each bar by different letters ($p<0.05$)

BPC1 is required for PRC2-mediated epigenetic suppression of camalexin pathway genes

Previous studies suggested that some BPC members closely interact with PRC2 complex components like FIE (FERTILIZATION-INDEPENDENT ENDOSPERM) and SWN (SWINGER) (Hecker et al. 2015; Xiao et al. 2017; Mu et al. 2017) which is required to epigenetically maintain the transcriptional suppression of downstream target genes via deposition of H3K27me3, a repressive histone mark (Mu et al. 2017; Hecker et al. 2015; Kooiker et al. 2005; Petrella et al. 2020). Furthermore, a recent study reported that multiple camalexin pathway genes were highly enriched with H3K27me3 (Zhao et al. 2021)., prompting us to interrogate publicly available Arabidopsis H3K27me3 ChIP-seq datasets (Wang et al. 2016; Cui et al. 2016). Among six up-regulated genes in *bpc1-1* mutant, three genes (*MYB51*, *CYP71A12*, and *CYP71B15*) were substantially enriched with H3K27me3 on their genomic regions (Fig. 4A), suggesting that their upregulation in *bpc1-1* might result from impaired PRC2-mediated silencing.

Because CLF and SWN catalyze the H3K27me3 on target loci, we examined publicly available ChIP-seq datasets comparing H3K27me3 enrichment between Col-0 and the *clf; swn* double mutant. In the *clf; swn* mutant, H3K27me3 enrichment at the *MYB51*, *CYP71A12*, and *CYP71B15* loci was substantially reduced (Fig. 4B). In addition, we conducted qRT-PCR analysis between Col-0 and *clf; swn*, a double mutant of the H3K27 methyltransferases *CLF* and *SWN*, which are core components of the *Arabidopsis* PRC2 complex. Transcript levels of the transcription factor,

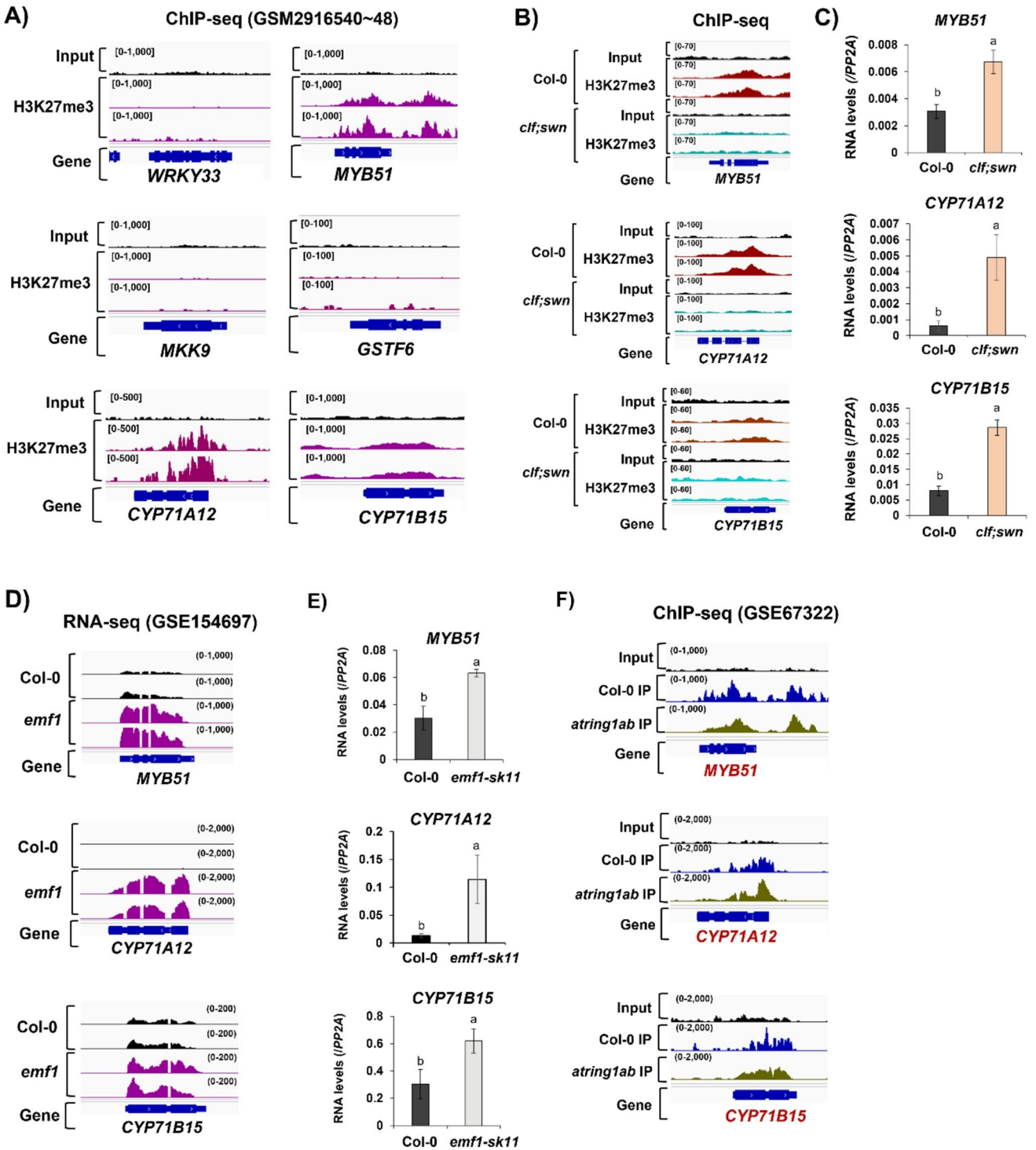

MYB51 and the camalexin biosynthetic genes, *CYP71A12* and *CYP71B15* were significantly increased in the *clf; swn* mutant compared with those in Col-0 (Fig. 4C), supporting a critical role for PRC2 in the repression of camalexin biosynthetic genes.

Next, we also analyzed a publicly available RNA-seq dataset (GSE154697) comparing wild-type Col-0 and the *emf1* mutant, a loss-of-function mutant of *EMBRYONIC FLOWER 1* (*EMF1*), another essential component of the Polycomb Repressive Complex 2 (PRC2). Consistent with the results obtained from the *clf; swn* mutant, the three H3K27me3-enriched genes, *MYB51*, *CYP71A12*, and *CYP71B15* which were de-repressed in both *bpc1-1* and *clf; swn* mutants were also significantly upregulated in the *emf1*

Fig. 4 Polycomb complexes suppress biosynthesis of camalexin. **A** IGV genomic browser viewer illustration showing enrichment of H3K27me3 on six camalexin pathway genes (*WRKY33*, *MYB51*, *CYP71A12*, *MKK9*, *GSTF6*, and *CYP71B15*) which were upregulated in *bpc1-1* mutant compared to Col-0. Three camalexin pathway genes like *MYB51*, *CYP71A12*, and *CYP71B15* were highly enriched with H3K27me3 histone mark in comparison to those of input DNA. Ranged numbers in bracket indicating the amplitude of the signal were shown at the left upper corner of individual track. Detailed information regarding the genome-wide data was provided in Supplementary Table S2. **B** IGV genomic browser viewer illustration showing enrichment of H3K27me3 levels of three camalexin pathway genes (*MYB51*, *CYP71A12*, and *CYP71B15*) between Col-0 wild type and the *clf; swn* double mutant. All examined three camalexin pathway genes exhibited significantly reduced levels of H3K27me3 in the *clf; swn* double mutant in comparison to those of Col-0 wild type. Ranged numbers in bracket indicating the amplitude of the signal were shown at the left upper corner of individual track. Detailed information regarding the genome-wide data was provided in Supplementary Table S2. **C** Result of qRT-PCR analysis on three camalexin pathway genes (*MYB51*, *CYP71A12*, and *CYP71B15*) between Col-0 and the *clf; swn* mutant, which were detected to be enriched with H3K27me3. The *clf; swn* mutant is a double mutant generated by crossing between *clf-sk81* (SALK_106381) and *swn-2* (SALK_010213). One-way ANOVA was applied to calculate the statistical significance, and significant difference was indicated in the figures by different letters ($p<0.05$). **D** Result of public available RNA-seq dataset between Col-0 and *emf1* mutant (GSE154697) on three camalexin pathway genes (*MYB51*, *CYP71A12*, and *CYP71B15*) which were densely enriched with H3K27me3. Ranged numbers in parenthesis indicating the amplitude of the signal were shown at the right upper corner of individual track. Detailed information regarding the genome-wide data was provided in Supplementary Table S2. **E** Result of qRT-PCR analysis on three camalexin pathway genes (*MYB51*, *CYP71A12*, and *CYP71B15*) between Col-0 and the *emf1-sk11* mutant (SALK_114383), a knock-out mutant of another PRC2 component, *EMF1*. One-way ANOVA was applied to calculate the statistical significance, and significant difference was indicated in the figures by different letters ($p<0.05$). **F** IGV genomic browser viewer illustration showing enrichment of H3K27me3 levels of three camalexin pathway genes (*MYB51*, *CYP71A12*, and *CYP71B15*) between Col-0 and the *atring1ab* double mutant. The *atring1ab* mutant is a double mutant of two essential components of PRC1 complex, *AtRING1A* and *AtRING1B*. Ranged numbers in parenthesis indicating the amplitude of the signal were shown at the left upper corner of individual track. Detailed information regarding the genome-wide data was provided in Supplementary Table S2. **G** Result of ChIP-qPCR analysis showing enrichment of H3K27me3 between Col-0, *bpc1-1* mutant, and two *pBPC1::BPC1-FLAG/bpc1-1* complementation lines (#2−1 and #9−3) on three camalexin pathway genes (*MYB51*, *CYP71A12*, and *CYP71B15*) using anti-H3K27me3 antibody. Level of H3K27me3 was markedly reduced in the *bpc1-1* mutant on three camalexin pathway genes (*MYB51*, *CYP71A12*, and *CYP71B15*) compared to those of Col-0. In addition, reduced level of H3K27me3 on three camalexin pathway genes in *bpc1-1* mutant was at least partially recovered in two *pBPC1::BPC1-FLAG/bpc1-1* complementation lines (#9−3 and #2−1). **H** Result of ChIP-qPCR analysis showing enrichment of BPC1-FLAG on three H3K27me3-enriched (*MYB51*, *CYP71A12*, and *CYP71B15*) and two H3K27me3-depleted (*MKK9* and *GSTF6*) genes. ChIP assay was conducted using anti-FLAG antibody (ab205606, Abcam, UK) between *bpc1-1* mutant and two *pBPC1::BPC1-FLAG/bpc1-1* complementation lines (#2−1 and #9−3). **G–H** Genomic structure of each camalexin pathway gene and location of PCR amplicon (indicated by red bar with PX labelling, X is Arabic number) used in the ChIP-qPCR was presented above individual graph. One-way ANOVA was applied to calculate the statistical significance, and significant difference was indicated in the figures by different letters ($p<0.05$)

mutant compared with Col-0 (Fig. 4D). This observation was further validated by qRT-PCR analysis between Col-0 and *emf1-sk11* mutant (Fig. 4E). These results indicate that the EMF1-containing PRC2 complex plays an important role in the repression of camalexin biosynthetic genes in *Arabidopsis*. Taken together, these results confirmed that PRC2-mediated H3K27me3 deposition is essentially required for repression of these camalexin pathway genes.

Given that PRC2 can function cooperatively with Polycomb Repressive Complex 1 (PRC1) at certain target loci, we further examined H3K27me3 enrichment in the *atring1a; atring1b* double mutant (*atring1ab*), which lacks two core PRC1 components, AtRING1A (ARABIDOPSIS THALIANA RING1A) and AtRING1B. No significant changes in H3K27me3 levels were detected at the *MYB51*, *CYP71A12*, or *CYP71B15* loci in this mutant (Fig. 4F), suggesting that PRC1 is not substantially involved in the regulation of camalexin biosynthetic genes. Collectively, these results demonstrate that camalexin pathway genes are epigenetically repressed by PRC2 complexes in *Arabidopsis* and that this repression operates independently of PRC1.

BPC1 directly regulates some camalexin pathway genes

BPC1, which encodes a GAGA-binding domain, has been shown to bind GA-rich (C-box) sequences (Kooiker et al. 2005). To investigate whether BPC1 directly targets camalexin biosynthetic genes, we analyzed the promoter regions of six camalexin pathway genes that were upregulated in the *bpc1-1* mutant. Notably, all six genes (*WRKY33*, *MYB51*, *MKK9*, *GSTF6*, *CYP71A12*, and *CYP71B15*) contained at least one GA-rich motif within their promoter regions (Supplementary Fig. S3), suggesting that BPC1 may directly recruit PRC2 to these loci to mediate H3K27me3 deposition.

To functionally validate the *bpc1-1* mutant phenotype, a complementation construct was generated comprising the native *BPC1* promoter (approximately 2 kb upstream of the transcription start site) driving the full-length *BPC1* coding sequence fused in-frame with a C-terminal FLAG tag. The resulting construct (*pBPC1::BPC1-FLAG*) was introduced into the *bpc1-1* mutant background by floral dip transformation to generate *pBPC1::BPC1-FLAG/bpc1-1* complementation lines. Two independent homozygous T_3 lines (#2−1 and #9−3) carrying a single-copy insertion were selected for further analyses. Quantification of camalexin levels showed that both transgenic lines exhibited a significant reduction in camalexin accumulation compared with the *bpc1-1* mutant, although levels did not fully return to those observed in Col-0 (Supplementary Fig. S4). Using these transgenic lines, we also performed ChIP-qPCR to examine H3K27me3 enrichment at three camalexin pathway genes

Fig. 5 Epigenetic activation marks are enriched at the*BPC1*locus. **A** IGV genome browser illustration showing diverse histone H3 methylations on *BPC1* locus. Multiple active histone modifications including H3K4me2, H3K4me3, H3K36me3 were densely enriched at the *BPC1* genomic region. Meanwhile, repressive marks like H3K9me2 and H3K27me3 are not detected in the *BPC1* locus compared to those of input DNA. Ranged numbers in bracket in y-axis on individual track indicate the amplitude of the signal. Detailed information regarding the genome-wide data was provided in Supplementary Table S2. **B** IGV genome browser illustration showing diverse histone H3 acetylations on *BPC1* locus. Multiple histone H3 acetylation (H3ac) like H3K9ac, H3K14ac, and H3K27ac were observed along the gene coding body, indicating an open and accessible chromatin state. Signal intensities represent mean enrichment values normalized to input controls. Ranged numbers in bracket at the right corner of each track indicate the amplitude of the signal. Detailed information regarding the genome-wide data was provided in Supplementary Table S2. **C** Result of qRT-PCR analysis between Col-0, *atx1-1* (a knock-out mutant of *ATX1*), *atx2-2* (a knock-out mutant of *ATX2*), *atx1;2* (*atx1-2;atx2-1*, CS71692) double mutant, *atx1;2;r7* (*atx1-2;atx2-1;atxr7-1*, CS71693), and *efs-3* (a knock-out mutant of *EFS*) mutants at 1-week-old seedling stages. One-way ANOVA with Tukey's post-hoc test was applied for statistical analysis. **D** Result of ChIP-qPCR analysis showing enrichment of H3K36me3 on *BPC1* region. ChIP assay was conducted using anti-H3K36me3 antibody (ab9050, Abcam, UK) between *Col-0* and *efs-3* mutant. Genomic structure of each camalexin pathway gene and location of PCR amplicon (indicated by red bar with PX labelling, X is Arabic number) used in the ChIP-qPCR was presented above individual graph. One-way ANOVA was applied to calculate the statistical significance, and significant difference was indicated in the figures by different letters ($p<0.05$). **E** Result of public ChIP-seq dataset of H3K36me3 (GSE92449). IGV genome browser illustration shows enrichment of H3K36me3 on *BPC1* locus between Col-0 and efs-3 mutant. Ranged numbers in bracket in y-axis on individual track indicate the amplitude of the signal. Detailed information regarding the genome-wide data was provided in Supplementary Table S2. **F** Result of public ChIP-seq dataset of H3K27ac (GSE80056). IGV genome browser illustration shows enriched level of H3K27ac mark on *BPC1* locus between Col-0 and *hda9-1* mutant. Highly elevated level of H3K27ac was detected in *hda9-1* mutant compared to that of Col-0. Input DNA and H3K27ac-immunoprecipitated DNA was presented with black and purple color, respectively. Ranged numbers in bracket in y-axis on individual track indicate the amplitude of the signal. Detailed information regarding the genome-wide data was provided in Supplementary Table S2. **G** Result of public ChIP-seq dataset of H3K9ac (GSE243403). IGV genome browser illustration shows enriched level of H3K9ac mark on *BPC1* locus between Col-0 and *hda9* mutant (SALK_007123). Elevated level of H3K9ac was detected in *hda9-1* mutant compared to that of Col-0. Input DNA and H3K9ac-immunoprecipitated DNA was presented with black and brownish yellow color, respectively. Ranged numbers in bracket in y-axis on individual track indicate the amplitude of the signal. Detailed information regarding the genome-wide data was provided in Supplementary Table S2. **H** Result of qRT-PCR analysis measuring transcript level of *BPC1* between Col-0 and *hda9-1* mutants at 1-week-old seedling stages. One-way ANOVA was applied to calculate the statistical significance, and significant difference was indicated in the figures by different letters ($p<0.05$). **I** Result of ChIP-qPCR analysis showing enrichment of HDA9-FLAG on *BPC1* region. ChIP assay was conducted using anti-FLAG antibody (ab205606, Abcam, UK) between *hda9-1* mutant and two *pHDA9::HDA9-FLAG/hda9-1* complementation lines (#4–6 and #6−5). Genomic structure of each camalexin pathway gene and location of PCR amplicon (indicated by red bar with PX labelling, X is Arabic number) used in the ChIP-qPCR was presented above individual graph. One-way ANOVA was applied to calculate the statistical significance, and significant difference was indicated in the figures by different letters ($p<0.05$). **J** A schematic model illustrating the functional role of BPC1 in regulating camalexin biosynthesis. The transcription of *BPC1* is epigenetically controlled and marked by strong enrichment of active histone modifications, including H3K4 and H3K36 methylation, deposited by histone methyltransferases such as ATX1, ATX2, ATXR7, and EFS. Multiple histone acetylation marks (H3K9ac, H3K14ac, and H3K27ac) are also present at the *BPC1* locus. In contrast, HDA9 may modulate *BPC1* expression dynamics by removing H3 acetylation. Once expressed, BPC1 functions as a repressor of camalexin biosynthesis by cooperating with the PRC2 complex, which catalyzes H3K27me3 deposition on downstream target genes. Within this regulatory framework, the BPC1–PRC2 module appears to directly suppress key components of the camalexin pathway, including the transcription factor *MYB51* and the biosynthetic enzyme genes, *CYP71A12* and *CYP71B15*. Through this mechanism, BPC1 contributes to the epigenetic repression of defense-related specialized metabolism, specifically camalexin production in *Arabidopsis*. BioRender (BioRender.com) was used to create this scientific illustration (license number: SR28W5QOCG)

(*MYB51*, *CYP71A12*, and *CYP71B15*). H3K27me3 levels at all three loci were markedly reduced in the *bpc1-1* mutant relative to Col-0, whereas partial restoration of H3K27me3 enrichment was observed in the *pBPC1::BPC1-FLAG/bpc1-1* lines (Fig. 4G), demonstrating that BPC1 is required for PRC2-mediated H3K27me3 deposition at these genes.

We further examined whether BPC1 directly binds to these loci by performing ChIP–qPCR using the FLAG-tagged BPC1 lines. Significant enrichment of BPC1-FLAG was detected at the *CYP71A12* and *CYP71B15* loci (Fig. 4H). In contrast, no detectable BPC1 binding was observed at *MYB51*, *MKK9*, or *GSTF6*. Notably, although H3K27me3 levels at *MYB51* were reduced in both *bpc1-1* and polycomb mutants, BPC1-FLAG binding at this locus was not detected under the conditions tested, possibly reflecting developmental or context-dependent regulation. Collectively, these results indicate that BPC1 negatively regulates camalexin production by directly binding to multiple camalexin biosynthetic genes and facilitating PRC2-mediated H3K27me3 deposition.

Expression of *BPC1* is epigenetically modulated by histone modification

To investigate the chromatin state of *BPC1*, we further analyzed multiple publicly available epigenome datasets showing enrichment of active histone marks as well as repressive histone marks in *Arabidopsis*. Integrative analysis revealed that the *BPC1* locus is consistently enriched with several histone marks associated with transcriptional activation (Fig. 5A). For instance, H3K4me2, H3K4me3, and H3K36me3 exhibited strong enrichment across the promoter and coding region of *BPC1* (Fig. 5A). Because of compact gene architecture of *BPC1*, the distribution of

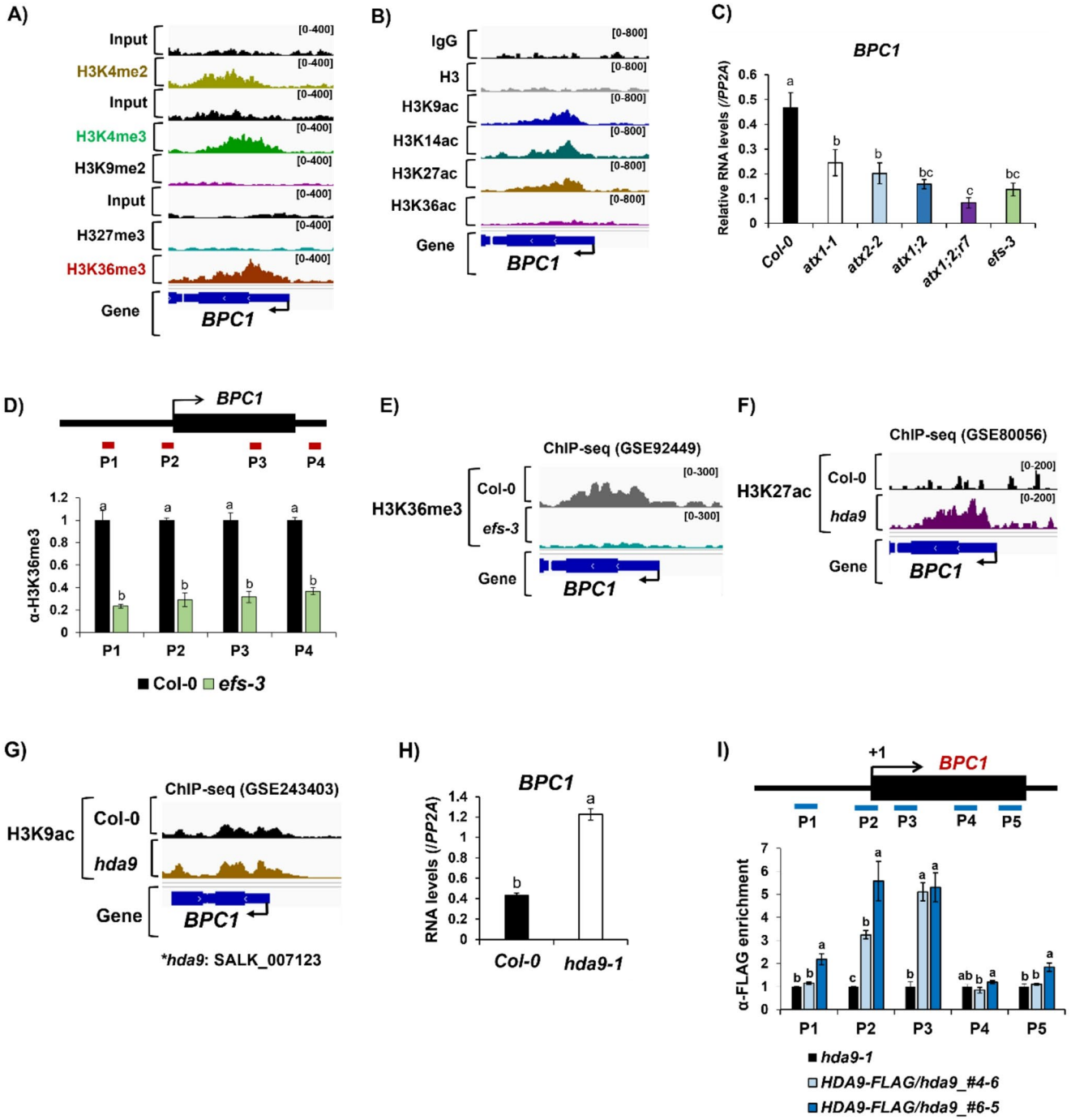

these active marks partially overlap, might results in a continuous active chromatin signature of *BPC1* locus. We also observed enrichment of multiple histone H3 acetylation (H3ac) like H3K9ac, H3K14ac, and H3K27ac at near transcription start site, further supporting the notion that *BPC1* might reside in an open and accessible chromatin environment (Fig. 5B). Meanwhile, we could not observe repressive histone marks like H3K9me2 and H3K27me3 on *BPC1* chromatin. Together, these epigenomic features indicate that *BPC1* is embedded within a highly active chromatin state characterized by H3K4 methylation, H3K36 trimethylation, and histone acetylation. This combination of active marks likely contributes to the stable and constitutive expression pattern of *BPC1* in most of tissues of *Arabidopsis* (Supplementary Fig. S5).

Histone H3K4 and H3K36 methylations in *Arabidopsis* are catalyzed by SET-domain containing methyltransferases such as ATX1 (ARABIDOPSIS TRITHORAX 1), ATX2, ATXR7 (ARABIDOPSIS TRITHORAX-RELATED7), and EFS (Alvarez-Venegas et al. 2006; Pien et al. 2008;

Tamada et al. 2009; Li et al. 2015). To determine whether these enzymes contribute to the transcriptional activation of *BPC1*, we conducted qRT-PCR analysis between Col-0 and a series of loss-of-function mutants like *atx1-2*, *atx2-1*, *atx1;atx2* double mutant, *atx1;atx2;atxr7* triple mutant, and *efs-3* mutant. As a result, *BPC1* transcript levels were significantly reduced in all tested mutants compared with wild-type Col-0 (Fig. 5C). Interestingly, *atx1;atx2* double and *atx1;atx;2;atxr7* triple mutant exhibited more pronounced reductions in *BPC1* expression than either the *atx1* or *atx2* single mutant, suggesting that ATX1, ATX2, and ATXR7 act redundantly to regulate *BPC1* expression.

BPC1 expression was also significantly reduced in *efs-3* mutant (Fig. 5C). EFS has been reported to promote transcriptional activation through the deposition of H3K36me3 at target loci (Li et al. 2015). Consistent with this function, ChIP–qPCR analysis revealed that H3K36me3 enrichment at the *BPC1* locus was substantially reduced in the *efs-3* mutant compared with Col-0 (Fig. 5D), correlating with decreased *BPC1* transcript level. This result was further supported by analysis of publicly available H3K36me3 ChIP-seq datasets, which showed strong H3K36me3 enrichment at the *BPC1* locus in Col-0 but pronounced depletion in the *efs-3* mutant (Fig. 5E).

Another group of histone H3K4 methyltransferases, including ATX3 (ARABIDOPSIS TRITHORAX 3), ATX4, and ATX5, has been reported to redundantly regulate gene expression through H3K4 di- and tri-methylation at numerous loci in *Arabidopsis* (Chen et al. 2017). To determine whether these enzymes are also involved in *BPC1* regulation, we analyzed publicly available H3K4me3 ChIP–seq datasets comparing Col-0 and the *atx3;atx4;atx5* (*atx3;4;5*) triple mutant. No significant differences in H3K4me3 enrichment were detected at the *BPC1* locus between Col-0 and the *atx3;4;5* mutant (Supplementary Fig. S6), suggesting that ATX3, ATX4, and ATX5 do not contribute to *BPC1* regulation. Taken together, these results demonstrate that ATX1, ATX2, and EFS promote active *BPC1* transcription by facilitating H3K4me3 and H3K36me3 deposition in *Arabidopsis*.

Given that *BPC1* chromatin is also enriched with multiple H3 acetylation marks, we next analyzed publicly available H3ac ChIP-seq datasets. We found that H3K27ac and H3K9ac levels at the *BPC1* locus were markedly elevated in the *hda9-1* mutant relative to Col-0 (Fig. 5F and G). Consistent with this, *BPC1* expression was significantly upregulated in *hda9-1* compared with the wild type (Fig. 5H). Furthermore, ChIP-qPCR analysis using *pHDA9::HDA9-FLAG/hda9-1* transgenic plants demonstrated that HDA9 directly associates with the *BPC1* genomic region (Fig. 5I). These findings indicate that HDA9 likely participates in the transcriptional modulation of *BPC1* by de-acetylating H3K9ac and H3K27ac at the *BPC1* locus. Collectively, these results demonstrate that *BPC1* transcription is epigenetically regulated through multiple active histone modifications and the chromatin-modifying enzymes that deposit or remove them.

Collectively, these findings enabled us to construct a schematic model illustrating the functional role of *BPC1* in regulating camalexin biosynthesis (Fig. 5I). The transcription of *BPC1* is epigenetically modulated and is characterized by strong enrichment of active histone marks, including H3K4 and H3K36 methylation, which are deposited by the histone methyltransferases like ATX1, ATX2, ATXR7 and EFS. Multiple histone acetylation marks are also present at the *BPC1* locus. In contrast, the histone deacetylase HDA9 appears to function as a negative regulator of *BPC1* expression by removing H3 acetylation from *BPC1* chromatin. Once expressed, BPC1 acts as a repressor of camalexin biosynthesis through its cooperation with the PRC2 complex, which catalyzes H3K27me3 deposition at downstream target genes. Within this regulatory framework, the BPC1-PRC2 module appears to directly suppress key components of the camalexin pathway, including the transcription factor, *MYB51* and the biosynthetic enzyme genes, *CYP71A12* and *CYP71B15*. Through this mechanism, BPC1 contributes to the epigenetic repression of defense-related specialized metabolism, camalexin in *Arabidopsis*.

Discussion

The results of this study uncover a previously unappreciated regulatory mechanism by which *BPC1* modulates camalexin biosynthesis through an epigenetically coordinated transcriptional network. Our transcriptome analysis demonstrated that *BPC1* specifically represses genes involved in camalexin biosynthesis, distinguishing its regulatory function from the partially overlapping, yet biologically distinct, role of its close homolog *BPC2*. The pronounced upregulation of multiple camalexin pathway genes in the *bpc1-1* mutant, together with elevated camalexin levels, clearly positions BPC1 as a key negative regulator of this specialized metabolic pathway.

To investigate the physical interactions between BPC1 and components of the PRC2 complex, we performed yeast two-hybrid (Y2H) assays. Under our experimental conditions, no interaction was detected between BPC1 and SWN or CLF. However, a weak but discernible interaction was observed between BPC1 and FIE (Supplementary Fig. S7). These results are partially consistent with Mu et al. (2017), which reported a BPC1-SWN interaction via Y2H and a BPC1-FIE interaction using bimolecular fluorescence complementation (BiFC) assay. The lack of a detectable

BPC1-SWN interaction in our study likely reflects differences in assay sensitivity or bait/prey configurations between the two systems, rather than an absence of biological interaction.

Several camalexin biosynthetic genes upregulated in *bpc1-1* exhibit strong H3K27me3 enrichment in wild-type plants, and these genes are de-repressed in PRC2 mutants, including *clf; swn* and *emf1* mutant (Fig. 4B and D). These observations indicate that PRC2-mediated H3K27me3 deposition plays an essential role in maintaining the suppressed state of camalexin biosynthetic genes under non-inducing conditions (Fig. 4G and H). Importantly, BPC1 directly binds GA-rich motifs within the genomic sequences of *CYP71A12* and *CYP71B15*, as demonstrated by ChIP-qPCR (Fig. 4H), possibly serving as a DNA-binding factor that helps recruit or stabilize PRC2 at these specific target loci. Although *MYB51* is also enriched with H3K27me3 and de-repressed in *bpc1-1* and PRC2 mutants, direct BPC1 binding at this locus was not detected under the conditions tested, suggesting that its regulation may be indirect or context-dependent. The absence of major H3K27me3 changes in the *atring1ab* PRC1 mutant further suggests that BPC1-dependent regulation of camalexin biosynthesis might operate primarily through PRC2 rather than PRC1 complex (Fig. 4F).

All molecular and epigenomic analyses in this study, including qRT-PCR, ChIP-qPCR and publicly available ChIP-seq datasets were conducted under standard, non-inducing growth conditions. Whether the BPC1-PRC2 module is dynamically remodeled upon pathogen challenge or elicitor treatment therefore remains an open question. Future studies employing targeted ChIP-qPCR for H3K27me3, H3K4me3, and histone acetylation marks at BPC1 target camalexin pathway loci under conditions of fungal infection or flg22 treatment would directly test whether stress-induced de-repression of camalexin biosynthetic genes is accompanied by loss of PRC2 occupancy or redistribution of active histone marks. Similarly, examining BPC1 chromatin occupancy via FLAG-based ChIP-qPCR in pathogen-challenged pBPC1::BPC1-FLAG transgenic lines would clarify whether BPC1 binding to GA-rich motifs at camalexin pathway gene promoters is attenuated during immune activation. Such experiments would help establish whether the BPC1-PRC2 repressive module is constitutively maintained or subject to signal-dependent release, providing a more complete picture of how epigenetic regulation is integrated with the rapid transcriptional induction of defense metabolism in Arabidopsis.

This study reveals that the transcription of *BPC1* itself is tightly controlled through a distinct layer of epigenetic regulation. The *BPC1* locus is enriched with multiple active histone marks, including H3K4me2, H3K4me3, H3K36me3, and H3 acetylation (Fig. 5A and B). Mutations in *ATX1*, *ATX2*, *ATXR7*, and *EFS*, histone methyltransferases responsible for H3K4 and H3K36 methylation significantly reduce *BPC1* expression (Fig. 5C), demonstrating that these marks contribute to maintaining the constitutive activation of *BPC1*. Conversely, loss of the histone deacetylase, HDA9 increases H3ac levels and elevates *BPC1* transcription, and HDA9 directly binds to the *BPC1* locus, indicating that HDA9 fine-tunes *BPC1* expression by counteracting histone acetylation (Fig. 5G and I). Thus, *BPC1* is regulated through an unusual arrangement in which multiple active histone modifications preserve its basal transcriptional activity, while de-acetylation by HDA9 modulates its expression dynamics.

The relatively constant expression of *BPC1* across tissues (Supplementary Fig. S5), together with its predicted interaction with PRC2, suggests that BPC1 may function as a stable epigenetic regulator that continuously modulates the physiological balance between growth and defense in plants. Because PRC2 catalyzes the deposition of H3K27me3 to repress transcription at target loci, a BPC1-PRC2 regulatory module could contribute to the sustained repression of defense-related metabolic genes under non-stress conditions. This model is consistent with the notion that the biosynthesis of defensive metabolites, such as camalexin, is energetically costly and therefore typically induced only upon exposure to biotic or abiotic stress. Nevertheless, we cannot exclude the possibility that *BPC1* expression might be dynamically regulated under specific environmental conditions (e.g., light/dark cycles), abiotic stresses (e.g., drought, salinity, or heat), or biotic challenges (e.g., pathogen infection or herbivory). Further studies are required to determine whether *BPC1* responds to specific stimuli in *Arabidopsis*.

Taken together, our findings support a model in which BPC1 functions as an epigenetically regulated transcriptional repressor that partners with PRC2 to suppress camalexin biosynthesis under basal (non-stressed) condition. This regulatory module integrates chromatin-based modulation of *BPC1* transcription with direct repression of downstream metabolic genes, ensuring that camalexin production remains tightly controlled under normal growth conditions. By preventing the unnecessary activation of such energetically demanding pathways, the BPC1-PRC2 module may contribute to optimizing the growth-defense balance by preventing unnecessary activation of defense pathways while maintaining the capacity for rapid induction under stress. Future work dissecting the environmental responsiveness of the BPC1-PRC2 module, as well as its interplay with other transcription factors and hormonal pathways, will further clarify how *Arabidopsis* coordinates specialized metabolism with physiological demands.

Materials and methods

Plant materials and growth conditions

Arabidopsis seeds were sterilized with 1.5% sodium hypochlorite (NaOCl) solution and stratified for 3 days at 4 ℃ in the dark. Then, stratified seeds were germinated and grown under long day condition (16-h light/8-h dark) at 22 ˚C in the growth room. The *bpc1-1* (CS68803), *bpc1-1;2 − 1* (CS68700), *clf-sk81* (SALK_106381), *swn-2* (SALK_010213), *atx1-2* (SALK_149002), *atx2-1* (SALK_117262), *hda9-1* (SALK_007123), *atx1-2;atx2-1* (CS71692), *atx1-2;atx2-1;atxr7-1* (CS71693) and *emf1-sk11* (SALK_114383) were purchased from the ABRC (Arabidopsis Biological Resource Center) and genotyped using genotyping primers (Supplementary Table S1). The *atx1-1* (Alvarez-Venegas et al. 2006) and *efs-3* (Kim et al. 2005) were previously reported.

Development of transgenic plants

For generation of *pBPC1::BPC1-FLAG/bpc1-1* transgenic line, genomic fragment of *BPC1* containing about 2 kb promoter and its full-length of coding sequence was amplified using Sol™ Pfu-X Taq DNA polymerase (SolGent, South Korea) and ligated into pENTR-D-TOPO vector (Thermo Fisher Scientific, USA). Sequence-confirmed *BPC1* in pENTR-D-TOPO vector was used for the transfer into the PW1357 plant expression vector which harbors 3xFLAG sequence at the C-terminal using LR clonase II enzyme (Thermo Fisher Scientific, USA). Sequence-verified construct was introduced into *Agrobacterium* strain *GV3101*, and then used to transform into *Arabidopsis* plants using floral dipping method (Clough and Bent 1998). The *pHDA9::HDA9-FLAG/hda9-1* transgenic line was previously reported (Choi et al. 2024). Transgenic plants were selected in a half-strength MS media containing appropriate antibiotics. Homozygous T_3 transgenic lines containing a single copy of transgene were selected and used for further molecular analyses including camalexin quantification analysis. Information on the primers used for development of transgenic lines were listed in the Supplementary Table S1.

RNA-seq library preparation and sequencing

Extraction of total RNAs were conducted using the RNeasy Plant Mini Kit (QIAGEN, USA) according to the manufacturer's instructions. The quantity and quality check of extracted RNAs were performed using a Nano-400 spectrophotometer (Allsheng Instrument Co., China). RNA-seq libraries were prepared using the TruSeq Stranded mRNA LT Sample Prep Kit (Illumina, Inc., USA). Sequencing was conducted using an Illumina NovaSeq6000 platform in the paired-end sequencing method (Macrogen Co., South Korea).

RNA-seq data analysis

Two-week-old seedlings grown under long-day photoperiod conditions (16 h light/8 h dark) were harvested in three independent biological replicates, and total RNA was extracted using the RNeasy Plant Mini Kit (QIAGEN, USA) according to the manufacturer's instructions. Raw fastq files were quality-checked using the FastQC program (www.bioinformatics.babraham.ac.uk/projects/fastqc/). Low quality of reads was filtered out using Trimmomatic (ver 0.36) prior to the mapping to the reference genome (Bolger et al. 2014). Trimmed high quality reads were only applied for mapping to *Arabidopsis* TAIR10 genome using STAR aligner with default parameters (Dobin et al. 2013). TAIR10 genome was downloaded from EnsemblPlants (https://plants.ensembl.org/Arabidopsis_thaliana/Info/Index). FeatureCounts were used for the conversion of aligned reads to digital counts (Liao et al. 2014). Differentially expressed genes between Col-0 and *bpc1-1* or Col-0 and *bpc1-1;bpc2-1* mutant were extracted using the edgeR program in the R (ver.3.6.1) (Robinson et al. 2010). Correlation heatmap were generated in the R packages (ver. 3.6.1). ShinyGO (ver 0.85) web-based tool (https://bioinformatics.sdstate.edu/go/) was used for GO analysis in this study (Ge et al. 2020). Expression heatmap data was generated using the MeV program (ver. 4.9.0; Howe et al. 2010). Aligned reads were converted to bigwig (bw) files to visualize in the platform of the Integrative Genomics Viewer (IGV) which was developed by the Broad Institute (Thorvaldsdottir et al. 2013).

Quantification of camalexin

Three biological replicates of Col-0 and *bpc1-1* seedlings were stratified at 4 °C for 2 days in darkness and subsequently grown for two weeks under long-day photoperiod conditions (16 h light/8 h dark). Two-week-old seedlings (200 mg fresh weight) were collected, immediately flash-frozen in liquid nitrogen, and stored at − 80 °C until extraction. Frozen tissue was ground to a fine powder under liquid nitrogen, extracted with 80% (v/v) methanol containing 0.1% formic acid (1 mL per sample) by vortexing for 30 min at 4 °C, and centrifuged at 13,000 × g for 10 min at 4 °C. Supernatants were filtered through a 0.22 µm PTFE membrane filter prior to injection. Camalexin was quantified using a Vanquish Core HPLC system (Thermo Fisher Scientific, USA) equipped with a Diode Array Detector (DAD) FG. Separation was achieved on an Agilent ZORBAX Eclipse XDB-C18 reversed-phase column using a gradient

mobile phase consisting of water with 0.1% formic acid (A) and methanol with 0.1% formic acid (B). The detector was set to monitor absorbance at 318 nm. Chromatographic data acquisition and quantitative analysis, including peak area integration, were performed using Chromeleon Chromatography Data System software (version 7.3; Thermo Fisher Scientific, USA). Concentrations were calculated from a standard curve prepared using authentic camalexin standard (Sigma-Aldrich, Cat. No. SML1016).

Total RNA extraction and quantitative real-time PCR (qRT-PCR) analysis

Two-week old seedlings were used for the extraction of total RNAs using RNeasy Plant mini kit (QIAGEN, USA). Residual DNA contamination was removed by the DNase I treatment (NEB, USA). Total 5 µg of purified total RNAs were used for the synthesis of cDNA using EasyScript reverse transcriptase (TransGen Biotech, China). Quantitative RT-PCR analysis was conducted using FastFACT™ Real-Time PCR Master Mix (BioFACT, Republic of Korea) in a LineGene 9600 Plus Real-Time PCR system (BioER, China). *PP2A* (AT1G13320) was used as a housekeeping gene for normalization (Czechowski et al. 2005). Three biological replicates were used for each qRT-PCR analysis. One-way ANOVA with Tukey's post-hoc test was applied for statistical analysis. Information on the primer sequences used in the qRT-PCR analysis were listed in the Supplementary Table S1.

Chromatin immunoprecipitation (ChIP)-qPCR analysis

Col-0, *bpc1-1* mutant, and *pBPC1::BPC1-3xFLAG/bpc1-1* transgenic lines were grown for two weeks under the long day photoperiod (16 h day:8 h night) and harvested for ChIP-qPCR analysis. Samples were directly cross-linked in 1% formaldehyde solution, then finely ground in liquid nitrogen. ChIP assays were performed as previously described (Kim and Sung 2017). Antibodies of anti-H3K27me3 (07-449, Millipore, USA), anti-H3K36me3 (ab9050, Abcam, UK), anti-FLAG (ab205606, Abcam, UK) were purchased and used for ChIP assay. Quantitative PCR (qPCR) analysis was performed using FastFACT™ Real-Time PCR Master Mix (BioFACT, Republic of Korea) on LineGene 9600 Plus (FQD-96 A) Real-Time PCR Detection System (BioER, China). Enrichment of each amplicon was first calculated based on comparison to Ct value of Input DNA sample. Next, relative enrichment was calculated by comparing the amplicon values of the housekeeping gene, *PP2A*. ChIP-qPCR analysis was conducted with three technical replicates from at least two biological replicates. Primers used for ChIP-qPCR analysis were listed in the Supplementary Table S1.

Public RNA-seq and ChIP-seq dataset analyses

Publicly RNA-seq and ChIP-seq dataset were obtained from the European Bioinformatics Institute database (https://www.ebi.ac.uk/). For the RNA-seq data analysis, bad FASTQ reads were trimmed and quality-filtered before aligning to the *A. thaliana* TAIR10 transcriptome. Alignment to *A. thaliana* TAIR10 genome was performed using STAR aligner (Dobin et al. 2013). For the ChIP-seq data analysis, Bowtie2 was first used for the mapping to *A. thaliana* TAIR10 reference genome (Langmead and Salzberg 2012). Next, MACS2 command was used for peak callings (Zhang et al., 2008 Genome Biology). Aligned reads were visualized using Integrative Genomics Viewer (IGV) (Thorvaldsdottir et al. 2013). Public RNA-seq and ChIP-seq dataset analyzed in this study were shown in Supplementary Table S2.

Yeast two-hybrid assay

To examine the interactions between BPC1 and the PRC2 components, FIE, SWN, and CLF, full-length cDNA of *BPC1* was cloned into the pDEST32 vector to generate a fusion with the GAL4 DNA-binding domain at the C-terminus, while full-length cDNAs of *FIE*, *SWN*, and *CLF* were individually cloned into the pDEST22 vector to generate fusions with the GAL4 activation domain at the C-terminus. Primers used for cloning are listed in Supplementary Table S1. All constructs were introduced into the yeast strain MaV203 following the manufacturer's protocol (ProQuest™ Two-Hybrid System; Invitrogen, Carlsbad, CA, USA). Successful transformants were selected on synthetic dropout medium lacking tryptophan (SD/−Trp) or leucine (SD/−Leu), respectively. Mated diploid cells were initially selected on SD/−Leu/−Trp (−LT) medium, and protein–protein interactions were subsequently assessed by plating selected colonies on SD/−Leu/−Trp/−His medium supplemented with 20 mM 3-amino-1,2,4-triazole (3-AT) (−LTH + 20 mM 3-AT). For interaction assays, yeast suspensions adjusted to OD_{600} = 0.8-1.0 were spotted in 10 µL aliquots and incubated at 30 °C for 4 days.

Statistical analysis

One-way ANOVA followed by Tukey's post hoc test ($p < 0.05$) was used to assess significant differences among mean values. Distinct lowercase letters above the bars indicate statistically significant differences. Error bars represent

standard deviations (±SD), reflecting the variability associated with each mean.

Supplementary Information The online version contains supplementary material available at https://doi.org/10.1007/s11103-026-01720-y.

Acknowledgements This study was supported by the Korea Forestry Promotion Institute (RS-2025-02213366) and by the National Research Foundation of Korea (RS-2025-16065991) to DHK.

Author contributions HM and DC prepared all plant materials and performed genetic and molecular experiments; DC and EC developed the transgenic plants and performed the ChIP-qPCR and HPLC analyses; ABND and HK analyzed the RNA-seq dataset; D-HK wrote the manuscript. Authors have reviewed and approved the final manuscript for submission.

Funding Open Access funding enabled and organized by Chung-Ang University

Data availability RNA-seq dataset analyzed in this study was deposited in the NCBI Gene Expression Omnibus with GEO accession code (GSE307463).

Declarations

Conflict of interest The authors declare no competing interests.

References

Alvarez-Venegas R, Sadder M, Hlavacka A, Baluska F, Xia Y, Lu G, Firsov A, Sarath G, Moriyama H, Dubrovsky JG, Avramova Z (2006) The Arabidopsis homolog of trithorax, ATX1, binds phosphatidylinositol 5-phosphate, and the two regulate a common set of target genes. Proc Natl Acad Sci U S A 103(15):6049–6054. https://doi.org/10.1073/pnas.0600944103

Blackledge NP, Klose RJ (2021) The molecular principles of gene regulation by Polycomb repressive complexes. Nat Rev Mol Cell Biol 22(12):815–833. https://doi.org/10.1038/s41580-021-00398-y

Bolger AM, Lohse M, Usadel B (2014) Trimmomatic: a flexible trimmer for Illumina sequence data. Bioinformatics. 30(15):2114-2120. https://doi.org/10.1093/bioinformatics/btu170

Bottcher C, Westphal L, Schmotz C, Prade E, Scheel D, Glawischnig E (2009) The multifunctional enzyme CYP71B15 (PHYTOALEXIN DEFICIENT3) converts cysteine-indole-3-acetonitrile to camalexin in the indole-3-acetonitrile metabolic network of Arabidopsis thaliana. Plant Cell 21(6):1830–1845. https://doi.org/10.1105/tpc.109.066670

Chen LQ, Luo JH, Cui ZH, Xue M, Wang L, Zhang XY, Pawlowski WP, He Y (2017) ATX3, ATX4, and ATX5 encode putative H3K4 methyltransferases and are critical for plant development. Plant Physiol 174(3):1795–1806. https://doi.org/10.1104/pp.16.01944

Choi D, Kim SH, Choi DM, Moon H, Kim JI, Huq E, Kim DH (2024) ELONGATED HYPOCOTYL 5 interacts with HISTONE DEACETYLASE 9 to suppress glucosinolate biosynthesis in Arabidopsis. Plant Physiol 196(2):1340–1355. https://doi.org/10.1093/plphys/kiae284

Clough SJ, Bent AF (1998) Floral dip: a simplified method for Agrobacterium-mediated transformation of Arabidopsis thaliana. Plant J 16(6):735–743. https://doi.org/10.1046/j.1365-313x.1998.00343.x

Cui X, Lu F, Qiu Q, Zhou B, Gu L, Zhang S, Kang Y, Cui X, Ma X, Yao Q, Ma J, Zhang X, Cao X (2016) REF6 recognizes a specific DNA sequence to demethylate H3K27me3 and regulate organ boundary formation in Arabidopsis. Nat Genet 48(6):694–699. https://doi.org/10.1038/ng.3556

Czechowski T, Stitt M, Altmann T, Udvardi MK, Scheible WR (2005) Genome-wide identification and testing of superior reference genes for transcript normalization in Arabidopsis. Plant Physiol 139(1):5–17. https://doi.org/10.1104/pp.105.063743

Dobin A, Davis CA, Schlesinger F, Drenkow J, Zaleski C, Jha S, Batut P, Chaisson M, Gingeras TR (2013) STAR: ultrafast universal RNA-seq aligner. Bioinformatics 29(1):15–21. https://doi.org/10.1093/bioinformatics/bts635

Ge SX, Jung D, Yao R (2020) ShinyGO: a graphical gene-set enrichment tool for animals and plants. Bioinformatics 36:2628–2629

Geu-Flores F, Moldrup ME, Bottcher C, Olsen CE, Scheel D, Halkier BA (2011) Cytosolic gamma-glutamyl peptidases process glutathione conjugates in the biosynthesis of glucosinolates and camalexin in Arabidopsis. Plant Cell 23(6):2456–2469. https://doi.org/10.1105/tpc.111.083998

Glawischnig E (2007) Camalexin. Phytochemistry 68(4):401–406. https://doi.org/10.1016/j.phytochem.2006.12.005

Hecker A, Brand LH, Peter S, Simoncello N, Kilian J, Harter K, Gaudin V, Wanke D (2015) The Arabidopsis GAGA-binding factor BASIC PENTACYSTEINE6 recruits the POLYCOMB-REPRESSIVE COMPLEX1 component LIKE HETEROCHROMATIN PROTEIN1 to GAGA DNA motifs. Plant Physiol 168(3):1013–1024. https://doi.org/10.1104/pp.15.00409

Howe E, Holton K, Nair S, Schlauch D, Sinha R, Quackenbush J (2010) MeV: Multi Experiment viewer. https://doi.org/10.1007/978-1-4419-5714-6_15

Kim DH, Sung S (2017) The Binding Specificity of the PHD-Finger Domain of VIN3 Moderates Vernalization Response. Plant Physiol 173(2):1258–1268. https://doi.org/10.1104/pp.16.01320

Kim SY, He Y, Jacob Y, Noh YS, Michaels S, Amasino R (2005) Establishment of the vernalization-responsive, winter-annual habit in Arabidopsis requires a putative histone H3 methyl transferase. Plant Cell 17(12):3301–3310. https://doi.org/10.1105/tpc.105.034645

Kim SY, Lee J, Eshed-Williams L, Zilberman D, Sung ZR (2012) EMF1 and PRC2 cooperate to repress key regulators of Arabidopsis development. Plos Genet 8(3):e1002512. https://doi.org/10.1371/journal.pgen.1002512

Kooiker M, Airoldi CA, Losa A, Manzotti PS, Finzi L, Kater MM, Colombo L (2005) BASIC PENTACYSTEINE1, a GA binding protein that induces conformational changes in the regulatory region of the homeotic Arabidopsis gene SEEDSTICK. Plant Cell 17(3):722–729. https://doi.org/10.1105/tpc.104.030130

Langmead B, Salzberg SL (2012) Fast gapped-read alignment with Bowtie 2. Nat Methods 9(4):357–U354. https://doi.org/10.1038/Nmeth.1923

Liao Y, Smyth GK, Shi W (2014) featureCounts: an efficient general purpose program for assigning sequence reads to genomic features. Bioinformatics 30(7):923–930. https://doi.org/10.1093/bioinformatics/btt656

Li Y, Mukherjee I, Thum KE, Tanurdzic M, Katari MS, Obertello M, Edwards MB, McCombie WR, Martienssen RA, Coruzzi GM (2015) The histone methyltransferase SDG8 mediates the epigenetic modification of light and carbon responsive genes in plants. Genome Biol 16(1):79. https://doi.org/10.1186/s13059-015-0640-2

Meister RJ, Williams LA, Monfared MM, Gallagher TL, Kraft EA, Nelson CG, Gasser CS (2004) Definition and interactions of a positive regulatory element of the Arabidopsis INNER NO OUTER promoter. Plant J 37(3):426–438. https://doi.org/10.1046/j.1365-313x.2003.01971.x

Merini W, Calonje M (2015) PRC1 is taking the lead in PcG repression. Plant J 83(1):110–120. https://doi.org/10.1111/tpj.12818

Millet YA, Danna CH, Clay NK, Songnuan W, Simon MD, Werck-Reichhart D, Ausubel FM (2010) Innate immune responses activated in Arabidopsis roots by microbe-associated molecular patterns. Plant Cell 22(3):973–990. https://doi.org/10.1105/tpc.109.069658

Molitor AM, Bu Z, Yu Y, Shen WH (2014) Arabidopsis AL PHD-PRC1 complexes promote seed germination through H3K4me3-to-H3K27me3 chromatin state switch in repression of seed developmental genes. Plos Genet 10(1):e1004091. https://doi.org/10.1371/journal.pgen.1004091

Monfared MM, Simon MK, Meister RJ, Roig-Villanova I, Kooiker M, Colombo L, Fletcher JC, Gasser CS (2011) Overlapping and antagonistic activities of BASIC PENTACYSTEINE genes affect a range of developmental processes in Arabidopsis. Plant J 66(6):1020–1031. https://doi.org/10.1111/j.1365-313X.2011.04562.x

Mu Y, Zou M, Sun X, He B, Xu X, Liu Y, Zhang L, Chi W (2017) BASIC PENTACYSTEINE proteins repress ABSCISIC ACID INSENSITIVE4 expression via direct recruitment of the polycomb-repressive complex 2 in arabidopsis root development. Plant Cell Physiol 58(3):607–621. https://doi.org/10.1093/pcp/pcx006

Nafisi M, Goregaoker S, Botanga CJ, Glawischnig E, Olsen CE, Halkier BA, Glazebrook J (2007) Arabidopsis cytochrome P450 monooxygenase 71A13 catalyzes the conversion of indole-3-acetaldoxime in camalexin synthesis. Plant Cell 19(6):2039–2052. https://doi.org/10.1105/tpc.107.051383

Petrella R, Caselli F, Roig-Villanova I, Vignati V, Chiara M, Ezquer I, Tadini L, Kater MM, Gregis V (2020) BPC transcription factors and a Polycomb Group protein confine the expression of the ovule identity gene SEEDSTICK in Arabidopsis. Plant J 102(3):582–599. https://doi.org/10.1111/tpj.14673

Pien S, Fleury D, Mylne JS, Crevillen P, Inze D, Avramova Z, Dean C, Grossniklaus U (2008) ARABIDOPSIS TRITHORAX1 dynamically regulates FLOWERING LOCUS C activation via histone 3 lysine 4 trimethylation. Plant Cell 20(3):580–588. https://doi.org/10.1105/tpc.108.058172

Robinson MD, McCarthy DJ, Smyth GK (2010) edgeR: a Bioconductor package for differential expression analysis of digital gene expression data. Bioinformatics 26(1):139–140. https://doi.org/10.1093/bioinformatics/btp616

Saga H, Ogawa T, Kai K, Suzuki H, Ogata Y, Sakurai N, Shibata D, Ohta D (2012) Identification and characterization of ANAC042, a transcription factor family gene involved in the regulation of camalexin biosynthesis in Arabidopsis. Mol Plant Microbe Interact 25(5):684–696. https://doi.org/10.1094/MPMI-09-11-0244

Sangwan I, O'Brian MR (2002) Identification of a soybean protein that interacts with GAGA element dinucleotide repeat DNA. Plant Physiol 129(4):1788–1794. https://doi.org/10.1104/pp.002618

Santi S, Schmidt W (2009) Dissecting iron deficiency-induced proton extrusion in Arabidopsis roots. New Phytol 183(4):1072–1084. https://doi.org/10.1111/j.1469-8137.2009.02908.x

Schubert D, Primavesi L, Bishopp A, Roberts G, Doonan J, Jenuwein T, Goodrich J (2006) Silencing by plant Polycomb-group genes requires dispersed trimethylation of histone H3 at lysine 27. EMBO J 25(19):4638–4649. https://doi.org/10.1038/sj.emboj.7601311

Schuhegger R, Nafisi M, Mansourova M, Petersen BL, Olsen CE, Svatos A, Halkier BA, Glawischnig E (2006) CYP71B15 (PAD3) catalyzes the final step in camalexin biosynthesis. Plant Physiol 141(4):1248–1254. https://doi.org/10.1104/pp.106.082024

Shanks CM, Hecker A, Cheng CY, Brand L, Collani S, Schmid M, Schaller GE, Wanke D, Harter K, Kieber JJ (2018) Role of BASIC PENTACYSTEINE transcription factors in a subset of cytokinin signaling responses. Plant J 95(3):458–473. https://doi.org/10.1111/tpj.13962

Shu J, Chen C, Thapa RK, Bian SM, Nguyen V, Yu KF, Yuan ZC, Liu J, Kohalmi SE, Li CL, Cui YH (2019) Genome-wide occupancy of histone H3K27 methyltransferases CURLY LEAF and SWINGER in Arabidopsis seedlings. Plant Direct 3(1). https://doi.org/10.1002/pld3.100

Simonini S, Roig-Villanova I, Gregis V, Colombo B, Colombo L, Kater MM (2012) Basic pentacysteine proteins mediate MADS domain complex binding to the DNA for tissue-specific expression of target genes in Arabidopsis. Plant Cell 24(10):4163–4172. https://doi.org/10.1105/tpc.112.103952

Su T, Xu J, Li Y, Lei L, Zhao L, Yang H, Feng J, Liu G, Ren D (2011) Glutathione-indole-3-acetonitrile is required for camalexin biosynthesis in *Arabidopsis thaliana*. Plant Cell 23(1):364–380. https://doi.org/10.1105/tpc.110.079145

Tamada Y, Yun JY, Woo SC, Amasino RM (2009) ARABIDOPSIS TRITHORAX-RELATED7 is required for methylation of lysine 4 of histone H3 and for transcriptional activation of FLOWERING LOCUS C. Plant Cell 21(10):3257–3269. https://doi.org/10.1105/tpc.109.070060

Theune ML, Bloss U, Brand LH, Ladwig F, Wanke D (2019) Phylogenetic analyses and GAGA-motif binding studies of BBR/BPC proteins lend to clues in GAGA-motif recognition and a regulatory role in brassinosteroid signaling. Front Plant Sci 10:466. https://doi.org/10.3389/fpls.2019.00466

Thorvaldsdottir H, Robinson JT, Mesirov JP (2013) Integrative Genomics Viewer (IGV): high-performance genomics data visualization and exploration. Brief Bioinform 14(2):178–192. https://doi.org/10.1093/bib/bbs017

Turck F, Roudier F, Farrona S, Martin-Magniette ML, Guillaume E, Buisine N, Gagnot S, Martienssen RA, Coupland G, Colot V (2007) Arabidopsis TFL2/LHP1 specifically associates with genes marked by trimethylation of histone H3 lysine 27. Plos Genet 3(6):e86. https://doi.org/10.1371/journal.pgen.0030086

Wang H, Liu C, Cheng J, Liu J, Zhang L, He C, Shen WH, Jin H, Xu L, Zhang Y (2016) Arabidopsis flower and embryo developmental genes are repressed in seedlings by different combinations of polycomb group proteins in association with distinct sets of cis-regulatory elements. Plos Genet 12(1):e1005771. https://doi.org/10.1371/journal.pgen.1005771

Xiao J, Jin R, Yu X, Shen M, Wagner JD, Pai A, Song C, Zhuang M, Klasfeld S, He C, Santos AM, Helliwell C, Pruneda-Paz JL, Kay SA, Lin X, Cui S, Garcia MF, Clarenz O, Goodrich J, Zhang X, Austin RS, Bonasio R, Wagner D (2017) Cis and trans determinants of epigenetic silencing by Polycomb repressive complex 2 in Arabidopsis. Nat Genet 49(10):1546–1552. https://doi.org/10.1038/ng.3937

Zhao K, Kong D, Jin B, Smolke CD, Rhee SY (2021) A novel bivalent chromatin associates with rapid induction of camalexin biosynthesis genes in response to a pathogen signal in Arabidopsis. Elife 10. https://doi.org/10.7554/eLife.69508

Zhou N, Tootle TL, Glazebrook J (1999) Arabidopsis PAD3, a gene required for camalexin biosynthesis, encodes a putative cytochrome P450 monooxygenase. Plant Cell 11(12):2419–2428. https://doi.org/10.1105/tpc.11.12.2419